Calculating Single-Channel Permeability and Conductance from Transition Paths

Xiaoyan Zhou[1,2] and Fangqiang Zhu[2,*]

[1]Department of Physics, Zhejiang Normal University, Jinhua 321004, China

[2]Department of Physics, Indiana University Purdue University Indianapolis, 402 North Blackford Street, Indianapolis, Indiana 46202, United States

[*] Correspondence: fzhu0@iupui.edu

This is the author's manuscript of the article published in final edited form as:
Zhou, X., & Zhu, F. (2019). Calculating Single-Channel Permeability and Conductance from Transition Paths. Journal of Chemical Information and Modeling. https://doi.org/10.1021/acs.jcim.8b00914

ABSTRACT

Permeability and conductance are the major transport property of membrane channels, quantifying the rate of channel crossing by the solute. It is highly desirable to calculate these quantities in all-atom molecular dynamics simulations. When the solute crossing rate is low, however, direct methods would require prohibitively long simulations, and one thus typically adopts alternative strategies based on the free energy of single solute along the channel. Here we present a new method to calculate the crossing rate by initiating unbiased trajectories in which the solute is released at the free energy barrier. In this method, the total time the solute spends in the barrier region during a channel crossing (transition path) is used to determine the kinetic rate. Our method achieves a significantly higher statistical accuracy than the classical reactive flux method, especially for diffusive barrier crossing. Our test on ion permeation through a carbon nanotube verifies that the method correctly predicts the crossing rate and reproduces the spontaneous crossing events as in long equilibrium simulations. The rigorous and efficient method here will be valuable for quantitatively connecting simulations to experimental measurement of membrane channels.

INTRODUCTION

Cell membranes create a barrier that separates the inside of the cell from the outside and prevents the passage of most hydrophilic molecules. Some membrane proteins, in the meantime, are designed to transport materials across this barrier. Channels, a major class of these transport proteins, form pores in the membrane and allow specific molecules to pass through.[1] Membrane channels are ubiquitous and play indispensable physiological roles in all living systems, from the uptake of nutrients to the transduction of neural signals.

The major transport property of a membrane channel is its permeability, which determines the net flux of solute through the channel under a concentration difference. For ion channels, the major characteristic is their conductance, which determines the ionic current under an applied transmembrane voltage. If the passages of individual ions are completely independent and not coupled to each other, the conductance of an ion channel at low voltages can be predicted from its permeability at equilibrium.[2]

Given the available atomic structures of many membrane channels, it is desirable to calculate their permeability or conductance from molecular dynamics (MD) simulations.[3, 4] Furthermore, it is of great interest to reveal in the simulations the full atomic details of how the solutes cross the channel. For membrane channels (such as those with large pores) with fast transport kinetics, both the permeability (conductance) and the crossing events can be directly obtained from straightforward MD simulations at equilibrium[2] or under an electrochemical potential[5-7]. For channels with small permeability or when the solute concentrations are low, however, the required simulation time to capture spontaneous permeation events can be very long. In such cases, it is often more efficient to first calculate a single-solute free energy profile, based on

which the permeability can be further estimated. For example, a diffusion model that incorporates the free energy and position-dependent diffusion coefficients[8] was applied to calculate the conductance of an ion channel.[9] Similar methods were recently proposed to calculate the permeability of lipid bilayers.[10, 11] Alternatively, the channel permeability can be rigorously calculated using the classical reactive flux method developed by Bennett and Chandler,[12] by releasing the solute at the free energy barrier and computing the transmission coefficient.[13] However, this method will become inefficient for diffusive barrier crossing,[12] when the solute re-crosses the free energy barrier many times before exiting the channel.

Based on earlier theories[14-16], we recently demonstrated a method[17] to calculate the rates of spontaneous barrier crossing, in a simulation setup essentially identical to that in the reactive flux method. However, although our method does not explicitly assume diffusive motions, it is much more efficient than the reactive flux method for the cases of diffusive barrier crossing. In this study, we propose computational protocols based on this method to calculate the permeability and conductance of membrane channels.

We test our proposed method by calculating ion permeability for carbon nanotubes (CNTs). CNTs with appropriate radii have been used as model systems for biological channels in a number of computational studies.[18-21] In addition to water transport, the permeation and selectivity of Na^+, K^+, and Cl^- ions were investigated for various CNTs in simulations.[22-25] Furthermore, CNTs have shown potential applications in desalination of seawater[26-28] and separation of ions[29, 30], which are contingent on their properties of selective ion transport or rejection. The conductance of individual CNTs or CNT membranes has also been experimentally measured for a variety of ions.[24, 31-35]

Pristine CNTs can be modified by adding functional groups to the surface, and such functionalization could significantly change their properties.[36-40] Using our proposed method, here we carry out MD simulations to calculate the K^+ permeability for a narrow (8,8) CNT (diameter ~1.1 nm) in its pristine and functionalized (by adding a carboxylate group) forms. In addition to validating our method, the simulations also quantify the effect of a single carboxylate group on the ion conductance of the CNT.

METHODS

In this section, we first present the theories and methods for calculating the channel permeability and conductance, and then describe our simulations for a test system of CNT.

Crossing rate, permeability, and conductance

Consider a single channel in a membrane that separates two reservoirs with equal concentration ρ of a certain solute. We define the equilibrium crossing rate, k_0, as the average number of solutes spontaneously crossing the channel in one direction per unit time. At equilibrium, the crossing rate for the other direction is also k_0. Clearly, k_0 is a function of the solute concentration ρ. Under sufficiently low concentrations such that the interactions between individual solute molecules can be ignored, k_0 will be linearly proportional to ρ.

When a concentration difference $\Delta\rho$ between the two reservoirs exists, there will be a net transport of the solute down the concentration gradient. If the concentrations are sufficiently low, the net solute flux through the channel, j, will be linearly proportional to $\Delta\rho$:

$$j = p_s \Delta\rho, \qquad (1)$$

where the linear coefficient, denoted as p_s here, can be defined as the single-channel permeability for the solute. We note that whereas the number flux j (s^{-1}) and number concentration ρ (cm^{-3}) are adopted here, in experiments the molar flux j/N_A (mol/s) and molar concentration $C \equiv \rho/N_A$ (mol/cm^3) are more commonly used, with N_A the Avogadro's number. Nevertheless, the permeability p_s (cm^3/s), defined as the ratio of the flux to the concentration difference, remains the same in both notations. Also, if the solutes may only cross the membrane through the channels, the single-channel permeability p_s here multiplied by the channel density

(in unit of cm^{-2}) in the membrane will give the commonly-used membrane permeability P_m (cm/s), which determines the per-area flux (mol/s·cm^2) through the membrane.

When the interaction between the solutes can be ignored, the motion of each individual solute molecule would not be affected by the presence or absence of other solutes in either reservoir. Consequently, the rate of crossing events from reservoir A to B is linearly proportional to the solute concentration in A, and the rate of crossing from B to A is linearly proportional to the concentration in B, with the linear coefficient corresponding to the permeability:

$$p_s = k_0/\rho. \qquad (2)$$

This equation relates the channel permeability p_s to the equilibrium crossing rate k_0 under symmetric solute concentrations.

For channels that conduct ions, the major experimental observable is the ionic current I under an applied transmembrane voltage V and a symmetric bulk ion concentration ρ. At sufficiently small V, the I-V relation will be linear, and the slope defines a constant single-channel conductance $\gamma \equiv I/V$. In fact, for many biological[41] or synthetic[42] ion channels, the linear Ohm's law can be valid up to voltages much higher than physiological membrane potentials (~80 mV). Importantly, although the conductance γ is a non-equilibrium property, our earlier theory[2] shows that γ can be predicted from the spontaneous ion crossings at equilibrium. In general, this linear response theory only applies for the net charge transport arising from all of the ions in the system.[2] Under sufficiently low ion concentrations, however, the crossings of individual ions will be independent of each other. In such single-ion conduction regime, we previously proved[2, 9] that the conductance arising from a given ion species is related to the equilibrium crossing rate:

$$\gamma = e^2 k_0/k_B T, \qquad (3)$$

where e is the charge of the ion, k_B the Boltzmann constant, and T the temperature. Equations 2 and 3 then indicate:

$$\gamma = \frac{e^2}{k_B T} p_s \rho. \qquad (4)$$

Therefore, when the ion concentration ρ is sufficiently low, the single-channel conductance γ will be linearly proportional to ρ, with the linear coefficient determined by the equilibrium permeability p_s.

We note that both the permeability (Eq. 2) and the conductance (Eq. 3) for a single channel at a low solute concentration are determined by the equilibrium crossing rate k_0, which is thus the key objective of our computational method presented below.

Free energy for single-solute crossing

For membrane channels with small permeability/conductance or under low solute concentrations, the crossing rate k_0 will be very small, and very long simulations will thus be needed to produce spontaneous crossing events and to directly obtain k_0. To overcome such difficulty, enhanced sampling techniques can be applied to calculate the thermodynamics and kinetics of single-solute crossing, and the first step is typically to calculate the free energy profile for a single "tagged" solute along the channel, as described below.

We assume that the membrane channel is aligned along the z-axis and located at the origin in the x-y plane. To properly sample the bulk region, the tagged solute is typically under a lateral restraint[9] $u(x,y)$ in the simulations. One such example is a flat-bottom harmonic potential:

$$u(x,y) = \begin{cases} 0 & \text{if } R \le R_0 \\ K_{xy}(R - R_0)^2/2 & \text{if } R > R_0 \end{cases}, \qquad (5)$$

where $R \equiv \sqrt{x^2 + y^2}$, and K_{xy} is the spring constant. The parameter R_0 should be chosen to be larger than the pore radius, such that the lateral restraint only acts to confine the tagged solute when it is in the bulk region but has no effect when inside the channel. The effective cross-sectional area due to the lateral restraint is defined as[9]

$$S = \iint \exp\left[- u(x,y)/k_B T \right] dx dy, \qquad (6)$$

which quantifies the accessible lateral area when the tagged solute is in the bulk.

In the presence of the lateral potential above, we can calculate a one-dimensional free energy $G(z)$ as a function of the z-coordinate of the tagged solute, using umbrella sampling or other methods. We assume that the vertical offset of $G(z)$ is set such that its flat baselines at the two ends (representing regions of bulk solution) are at the zero level. We previously proved[9] that under a symmetric bulk solute concentration ρ that is sufficiently low, the one-dimensional equilibrium solute density (occupancy) $p_0(z)$ along the channel is related to the free energy of the tagged solute:

$$p_0(z) = \rho S \exp\left[- G(z)/k_B T \right]. \qquad (7)$$

$p_0(z)$ provides the equilibrium probability density for finding a solute molecule at the given vertical position z in the channel region. We note that the choice of the lateral potential $u(x,y)$ will affect the values of both $G(z)$ and S, but will not affect[9] the equilibrium density $p_0(z)$ in the pore region where the tagged solute always experiences a zero $u(x,y)$.

Rate calculation

The crossing rate can be calculated using our recent method[17] from pairs of unbiased forward and backward simulations with the tagged solute molecule initially at the free energy barrier. The

two simulations in each pair start with identical coordinates and reverted velocities for all the atoms. If the solute molecule exits to opposite sides of the membrane in the two simulations, the two trajectories will form a transition path (or reactive trajectory) that represents a spontaneous crossing event. Given any interval $[z_1,z_2]$ in the channel region, we define the duration $\tau(z_1,z_2)$ for a transition path as the total time the trajectory spends in the interval.[17] If the transition path visits the interval $[z_1,z_2]$ multiple times, $\tau(z_1,z_2)$ should be the sum of all the individual durations. Furthermore, each pair of the forward/backward simulations is associated with a kinetic factor λ defined as[17]

$$\lambda(z_1,z_2) = \begin{cases} 1/\tau(z_1,z_2) & \text{for transition path} \\ 0 & \text{otherwise} \end{cases}. \qquad (8)$$

According to this definition, if the two trajectories form a transition path, λ will be the inverse duration. In contrast, λ will be zero if the solute molecule exits to the same side of the channel in the two simulations (thus not forming a transition path).

Accordingly to our theory,[17] the crossing rate is related to the average λ value and the equilibrium occupancies:

$$k_0 = \frac{1}{2}P(z_1 \le z \le z_2) \cdot \langle \lambda(z_1,z_2) \rangle_{z_1 \le z \le z_2}. \qquad (9)$$

Here $P(z_1 \le z \le z_2) = \int_{z_1}^{z_2} p_0(z)dz$ is the equilibrium probability of finding a solute in the interval $[z_1,z_2]$ and can be obtained (Eq. 7) from the free energy discussed earlier. The expected value $\langle \lambda(z_1,z_2) \rangle_{z_1 \le z \le z_2}$ can be estimated by averaging over the $\lambda(z_1,z_2)$ values from all the forward/backward simulation pairs described above. Importantly, Eq. 9 requires that the initial coordinates of these unbiased simulations be drawn from the equilibrium distribution when the

solute is in the interval $[z_1,z_2]$.[17] These initial coordinates can be sampled from a simulation with the solute confined in $[z_1,z_2]$ by a flat-bottom potential such that the equilibrium distribution of the microstates within $[z_1,z_2]$ is preserved. Due to the independence of velocity distribution, the initial velocities for all the atoms (including the solute atoms) in the forward simulation can be taken from the sampling simulation above or simply assigned randomly according to the Maxwell–Boltzmann distribution. Then these velocities should be reverted and used as the initial atomic velocities in the backward simulation. Although Eq. 9 is valid for any $[z_1,z_2]$, choosing the interval in the barrier region of the free energy would result in a higher fraction of the transition paths, thus making the calculation more efficient. Combining Eq. 9 with Eqs. 2 and 7, we obtain an expression for the single-channel permeability:

$$p_s = \frac{1}{2}\langle\lambda(z_1,z_2)\rangle_{z_1 \le z \le z_2} \cdot S \cdot \int_{z_1}^{z_2} \exp\left[-G(z)/k_BT\right]dz. \qquad (10)$$

For ion channels, the conductance under an ion concentration ρ can then be obtained from Eq. 4.

If we choose an interval $[z_0 - \delta z/2, z_0 + \delta z/2]$ centered at z_0 and with a sufficiently small width δz, Eq. 9 can be expressed in a slightly simplified form:[17]

$$k_0 = \frac{1}{2}p_0(z_0) \cdot \delta z \cdot \left\langle\lambda\left(z_0 - \frac{\delta z}{2}, z_0 + \frac{\delta z}{2}\right)\right\rangle_{z_0},$$

or

$$k_0 = \frac{1}{2}\rho S \exp\left[-G(z_0)/k_BT\right] \cdot \delta z \cdot \left\langle\lambda\left(z_0 - \frac{\delta z}{2}, z_0 + \frac{\delta z}{2}\right)\right\rangle_{z_0}. \qquad (11)$$

Here the unbiased simulations for evaluating the $\langle\lambda\rangle$ should start with the solute at close vicinity of z_0. As mentioned earlier, it is preferable to choose z_0 at the barrier top of the free energy.

With the obtained k_0, the single-channel permeability or conductance can then be calculated using Eq. 2 or 3.

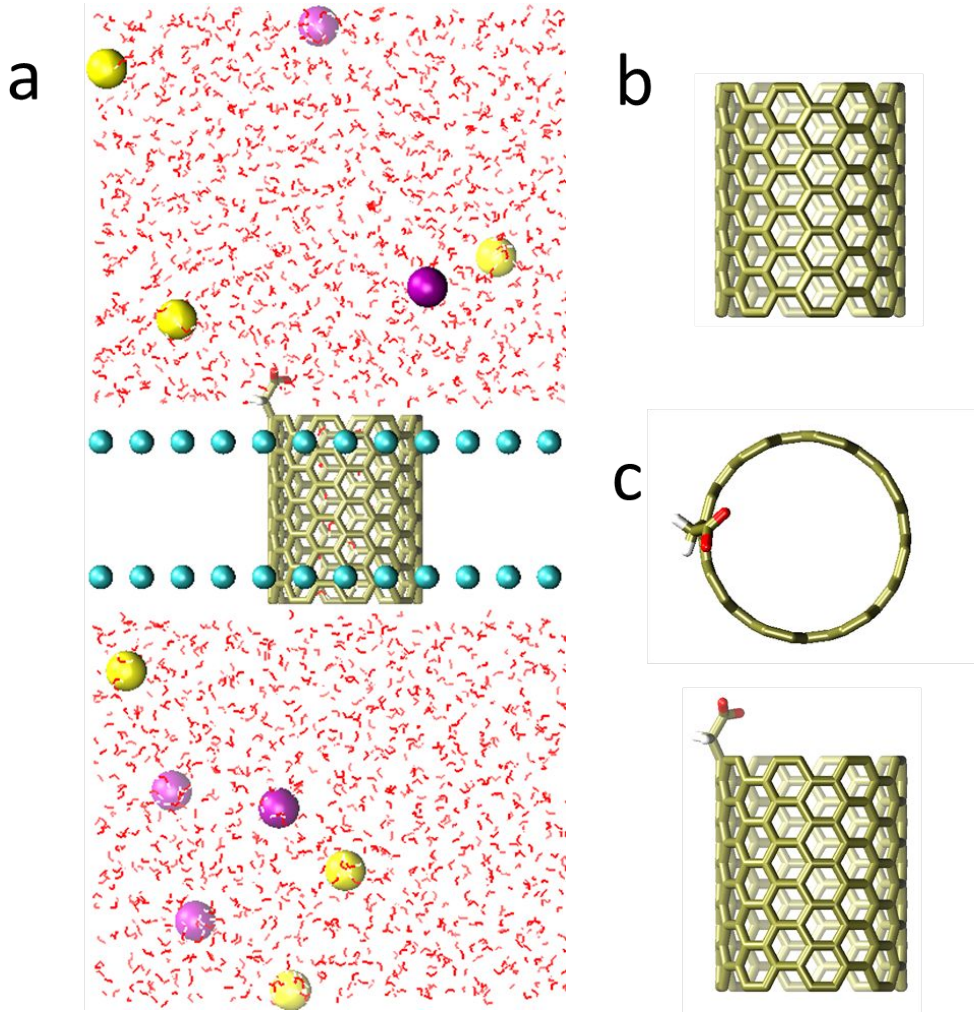

Figure 1. (a) Simulation system, consisting of two sheets of fixed carbon atoms serving as a membrane, a CNT channel, water molecules, and ions (K^+ in yellow and Cl^- in purple). (b) CNT0, a pristine (8,8) CNT. (c) The top and side views of CNT1, functionalized with a COO^- group.

Computational details

The simulation setup is shown in Fig.1. An uncapped (8,8) armchair CNT with 13.5 Å in length and 10.8 Å in diameter is located at the origin and aligned along the *z*-axis, between two carbon sheets that form an artificial membrane separating the solutions on the two sides. Two CNT

systems are studied in this work. The first system (denoted as CNT0) is a pristine CNT, and the second system (denoted as CNT1) has a functional (carboxylate COO^-) group at the edge. The solution contains 6 K^+ ions and 6 or 5 Cl^- ions in the CNT0 or CNT1 system, respectively, representing a bulk KCl concentration of about 130 mM. The CNT atoms and the membrane are fixed in all simulations, whereas the attached carboxylate group in CNT1 is free to move.

Simulation parameters were taken from an early version of the CHARMM22 force field[43] with the TIP3P water model[44], without the more recent calibration[45] for the K^+-Cl^- interaction parameters. The parameters for the CNT atoms here are identical to those in the up-to-date CHARMM force field, which reasonably reproduced the experimental adsorption affinities of many small molecules on CNTs.[46] All MD simulations were performed using the NAMD2 program[47] with a time step of 1 fs and under constant volume. Periodic boundary conditions were imposed with the unit cell size $36\,\text{Å} \times 36\,\text{Å} \times 73.5\,\text{Å}$. Unless noted otherwise, a constant temperature (300 K) was maintained by Langevin dynamics. The Particle Mesh Ewald (PME)[48] summation was used with a grid size of 1 Å for long-range electrostatic interactions. The van der Waals interactions were calculated with a cutoff distance of 12 Å.

Umbrella sampling simulations. For both the CNT0 and CNT1 systems, we took the z-coordinate of a K^+ ion as the reaction coordinate, and employed a total of 55 umbrella windows that cover the range $-27\,\text{Å} \le z \le 27\,\text{Å}$ with a constant spacing of 1 Å. In each simulation, the z-coordinate of the tagged K^+ ion was subject to a harmonic restraint with spring constant $K = 2.5\,\text{kcal}\cdot\text{mol}^{-1}\cdot\text{Å}^{-2}$. In addition, a lateral restraint $u(x,y)$ is applied in the x-y plane according to Eq. 5 with $K_{xy} = 10\,\text{kcal}\cdot\text{mol}^{-1}\cdot\text{Å}^{-2}$ and $R_0 = 6$ Å. We also adopted Hamiltonian replica exchange[49] in which a swap between the neighboring windows was attempted every 200 fs. The exchanges allowed the ion in each individual simulation (replica) to

move along the *z*-direction and could facilitate the equilibration of the orthogonal degrees of freedom.[9] The simulation for each window was run for 20 ns, and the coordinate of the tagged ion was recorded every time step. The first 2 ns of each simulation was discarded and the rest of the trajectory was used to calculate the free energy.

Unbiased simulations at barrier top. For the purpose of rate calculation, we performed forward and backward unbiased simulations at the free energy barrier as described below. First, 10 frames were selected from the umbrella sampling trajectories where the tagged ion is near the barrier at z = 0 Å. Next, starting from each frame, we performed a simulation of 20 ns in which the tagged K^+ ion was strongly restrained (200 kcal/mol/Å^2) at z = 0 Å, and then uniformly (every 2 ns) sampled 10 frames of atomic coordinates and velocities from the trajectory. Therefore, we obtained a total of 100 microstates from the 10 simulations. For each microstate, we further generated a companion microstate by reverting the velocities of all atoms in the system while keeping all the atomic positions unchanged. Finally, starting from each of these 200 microstates, we carried out a simulation of 1 ns without any restraint on the ion. In total, we thus performed 100 pairs of unbiased simulations with the tagged K^+ ion initially at z = 0 Å. Importantly, the two simulations in each pair started with identical coordinates but opposite velocities for all the atoms. To enable time reversibility, these unbiased simulations were under constant-NVE condition.

RESULTS

We tested our method by calculating ion permeability for two carbon nanotubes, CNT0 and CNT1, as described in Methods. First, for the thermodynamics, we performed umbrella sampling simulations with Hamiltonian replica exchange[49]. For each system, the free energy profile $G(z)$ (Fig. 2) as a function of the z-coordinate of a tagged K^+ ion was calculated from the umbrella sampling trajectories, using a fast numerical algorithm[50] of the weighted histogram analysis method[51]. By evaluating the variances of the mean forces,[50] the statistical errors in the calculated free energies are estimated to be about 0.1 kcal/mol, according to the established method.[50] In both cases, the free energies exhibit a relatively broad barrier inside the CNT, as shown in Fig. 2. The free energy profile for CNT0 is highly symmetric with respect to the center ($z = 0$ Å), as expected for a symmetric pore. In contrast, CNT1 features an energy well near the entrance where the attractive COO^- group[24, 38] is located.

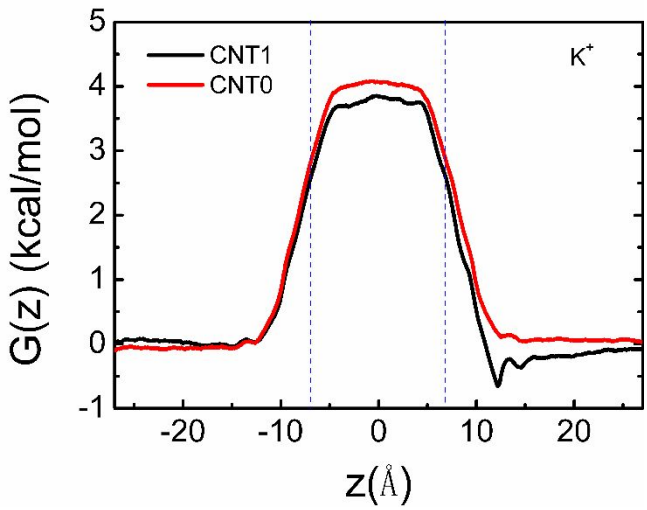

Figure 2. The calculated free energy profiles $G(z)$ for the tagged K^+ ion in the CNT0 and the CNT1 systems. The dashed lines indicate the length of the CNT.

We further calculated the kinetics by initiating forward and backward trajectories at the free energy barrier. For both CNT0 and CNT1, the highest free energies (Fig. 2) are found near the center of the CNT ($z = 0$ Å). For each system, therefore, we performed 100 pairs of unbiased simulations with the tagged ion initially at the CNT center. The ion exited the CNT within 1 ns in all of these simulations. In about one half of the simulation pairs, the ion exited opposite entrances of the CNT in the forward and backward simulations, thus forming a transition path (reactive trajectory). The ~50% fraction (Table 1) of transition paths among all the forward/backward trajectory pairs is consistent with diffusive barrier crossing, and also indicates that the z-coordinate of the tagged ion is a good reaction coordinate for the relatively simple systems here.

Table 1. Simulation results for the CNT0 and CNT1 systems.

						At 130 mM	
	$\boldsymbol{G(0)}$ kcal/mol	$\boldsymbol{N_{sim}}$	$\boldsymbol{N_{TP}}$	$\boldsymbol{\delta z \cdot \langle \lambda \rangle}$ m/s	$\boldsymbol{p_s}$ cm^3/s	$\boldsymbol{k_0}$ /s	$\boldsymbol{\gamma}$ pS
CNT0	4.1±0.1	100	50	3.8±0.9	(2.5±0.7)×10^{-15}	(2.0±0.6)×10^5	1.2±0.3
CNT1	3.8±0.1	100	52	3.7±1.1	(3.6±1.2)×10^{-15}	(2.8±1.0)×10^5	1.8±0.6

$G(0)$ is the value of the free energy $G(z)$ at z = 0 Å. N_{sim} is the total number of simulation pairs with the tagged ion released at z = 0 Å. N_{TP} is the number of simulation pairs in which the ion in the forward/backward trajectories exited opposite ends of the CNT, thus forming a transition path. $\langle \lambda \rangle$ is estimated by averaging over the λ values (defined in Eq. 8) from all the simulation pairs, for the interval [-0.1 Å, 0.1 Å] with $\delta z = 0.2$ Å. The permeability p_s is calculated (Eqs. 2 and 11) as $p_s = \frac{1}{2} S \exp\left[-G(0)/k_B T \right] \cdot \delta z \cdot \langle \lambda \rangle$. The spontaneous crossing rate k_0 and the conductance γ (in picosiemens) at a bulk ion concentration of 130 mM are further obtained from Eqs. 2 and 4, respectively.

We then analyzed the statistics of the obtained transition paths. First, we calculated the duration each transition path spent in a small interval [-0.1 Å, 0.1 Å] at the barrier. These durations, as shown in Fig. 3, are much longer than would be expected for a ballistic crossing, thus indicating the diffusive nature of the ion motions. We also calculated the total length of each

transition path, defined as the duration between the instants the ion enters and exits the CNT. Figure 3 shows that the lengths of transition path, or the durations of entire crossing event, range from 50 ps to 700 ps, with the most probable values around 175 ps. Overall, the durations in CNT1 are slightly longer than in CNT0. As mentioned before, each transition path formed by the forward/backward trajectories represents a spontaneous solute crossing and records all the atomic details therein. Figure 4 shows three snapshots in one of the transition paths of CNT1. The (8,8) CNT[28] is wide enough to accommodate multiple columns of H-bonded water molecules[22, 52]. Consequently, the K^+ ion is still coordinated by ~6 water molecules as it crosses the CNT, thus only experiencing a relatively moderate energetic barrier. Furthermore, the orientations of the water molecules (Fig. 4) are reversed when the ion traverses the CNT from one end to the other, as the water dipoles tend to point away from the cation.

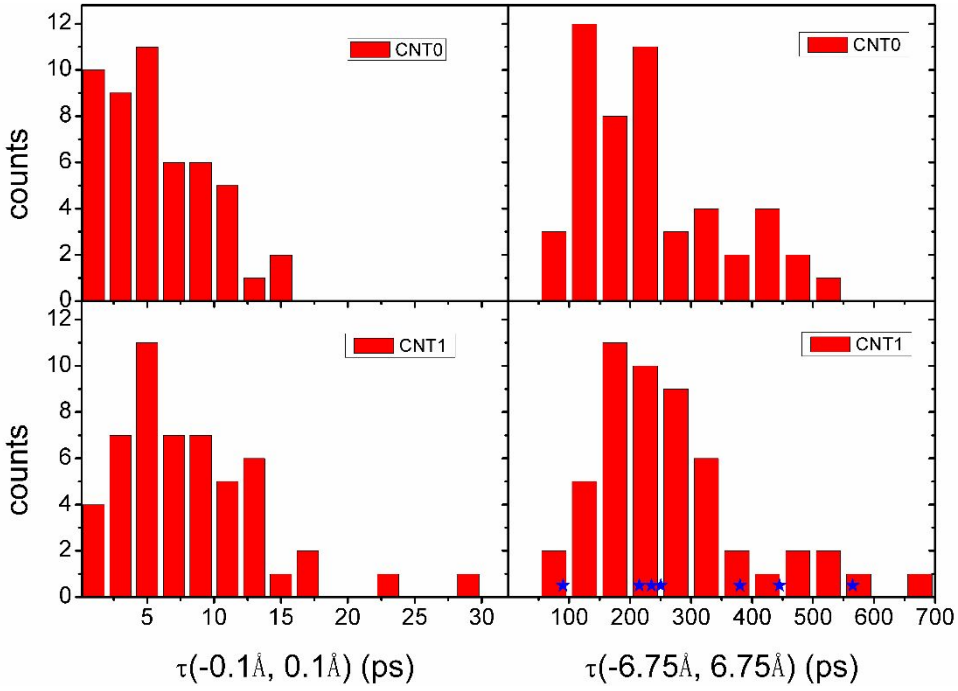

Figure 3. Statistics for the 50 and 52 transition paths from the CNT0 and CNT1 simulations, respectively. *Left*: histograms for the duration of the transition path in a small interval [-0.1 Å, 0.1 Å]. *Right*: histograms for the total length of the transition path, i.e., the duration in the entire 13.5 Å-long CNT. The 7 stars indicate the durations of the spontaneous crossing events in the long (2 μs) equilibrium simulations of CNT1.

From the durations of the transition paths in the small interval [-0.1 Å, 0.1 Å] of width $\delta z = 0.2$ Å, we calculated the average λ value (Eq. 8) over the 100 simulation pairs, with the results reported in Table 1. Furthermore, from the calculated $G(z)$ (Fig. 2), we obtained the value $G(z = 0)$ at the free energy barrier (Table 1). In addition, according to Eqs. 5 and 6, the lateral restraint ($K_{xy} = 10$ kcal $\cdot$ mol$^{-1} \cdot$ Å^{-2}, $R_0 = 6$ Å) applied in the umbrella sampling simulations corresponds to an effective cross-sectional area $S \approx 125$ Å^2. The permeability p_s for the CNT was then calculated (Table 1) according to Eqs. 2 and 11. The spontaneous crossing rate k_0 and the conductance γ depend on the bulk ion concentration, and their values at a concentration of 130 mM (corresponding to a number density $\rho = 7.83 \times 10^{-5}$/Å^3) are given in Table 1.

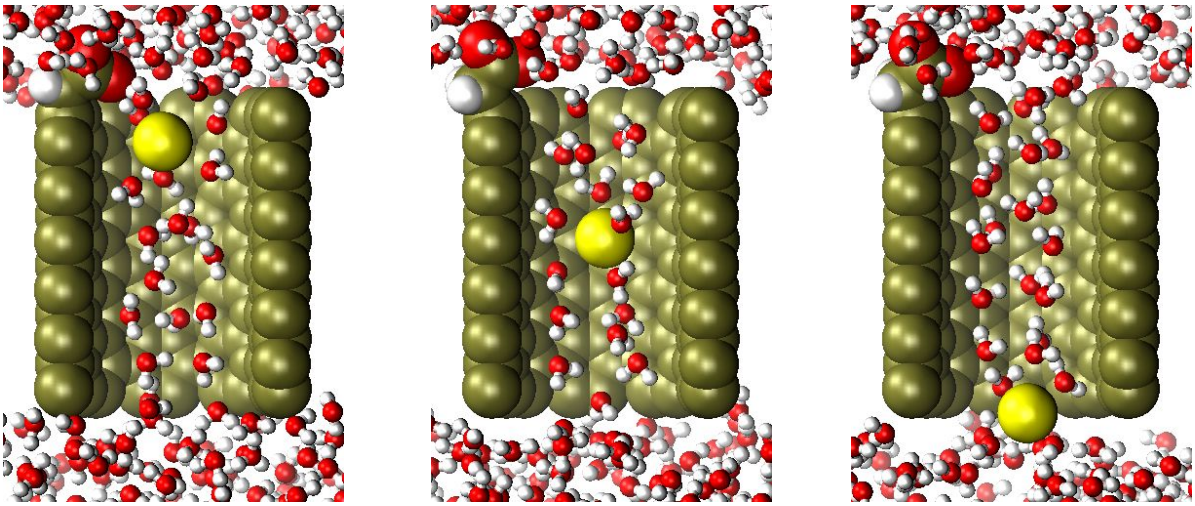

Figure 4. Snapshots (rendered in VMD[53]) of the tagged K^+ ion and water molecules in CNT1, taken from a transition path formed by forward/backward trajectories.

To verify the calculated kinetics, we performed long equilibrium simulations on a CNT1 system with 48 K^+ and 47 Cl^- ions corresponding to a bulk concentration of 1 M. For this system, we performed 10 independent equilibrium simulations without any restraint, each lasting 200 ns. During the total simulation time of 2 μs, we observed 6 spontaneous crossing events in

the $+z$ direction and 1 crossing event in the $-z$ direction for the K^+ ions, and no crossing for the Cl^- ions. Therefore, the K^+ crossing rate in these equilibrium simulations is k_0= 1.8±1.3 /μs. In comparison, at a concentration of 1 M (or $\rho = 6.02\times10^{-4}$ /Å^3), the crossing rate predicted from our calculated permeability (Table 1) of CNT1 is k_0 = 2.2±0.7 /μs. We note that the prediction is under the assumption that the crossing rate k_0 is linearly proportional to the bulk ion concentration ρ (Eq. 2), which may not be accurate for our case here with a relatively high ion concentration. Nevertheless, our predicted and observed crossing rates appear to agree reasonably well. Furthermore, the seven spontaneous crossing events in these long equilibrium simulations appear similar to those produced by the forward/backward trajectories initiated at the barrier top (Fig. 4). In particular, the durations of the seven crossing events here (Fig. 3) are consistent with the length distribution of the transition paths obtained from the forward/backward trajectories. Therefore, the combination of the free energy calculation and the unbiased simulations at the barrier top could faithfully reproduce the kinetic rates and the atomic details of the spontaneous solute crossing in long equilibrium simulations.

As an alternative approach, we also applied a diffusion model to calculate the single-channel permeability. To obtain the diffusivity, we performed additional umbrella sampling simulations, 5 ns per window, without Hamiltonian replica exchange. The trajectory of the ion under the constant harmonic potential in each window could then reveal the local diffusivity there. Specifically, we calculated the diffusion coefficient from the position autocorrelation time,[8] which was estimated from the variance of the mean position in the trajectory, as described in our previous study.[9] The estimated local diffusion coefficients as well as the values after a curve smoothing are shown in Fig. 5. The diffusion coefficients inside the hydrophobic CNTs here are about one half of the bulk values. In comparison, our previous study revealed that for a more

hydrophilic protein channel, the diffusion coefficients were reduced to much lower values.[9] Indeed, the diffusion coefficients near the attractive COO^- group in CNT1 here are also smaller than at other locations. As similarly done before,[9] from the free energy $G(z)$ (Fig. 2) and the diffusion coefficients $D(z)$, we calculated the single-channel permeability based on the Smoluchowski equation. The permeability p_s obtained using this approach is 1.6×10^{-15} cm^3/s for CNT0 and 2.1×10^{-15} cm^3/s for CNT1, in general agreement with the values (Table 1) calculated from the transition paths.

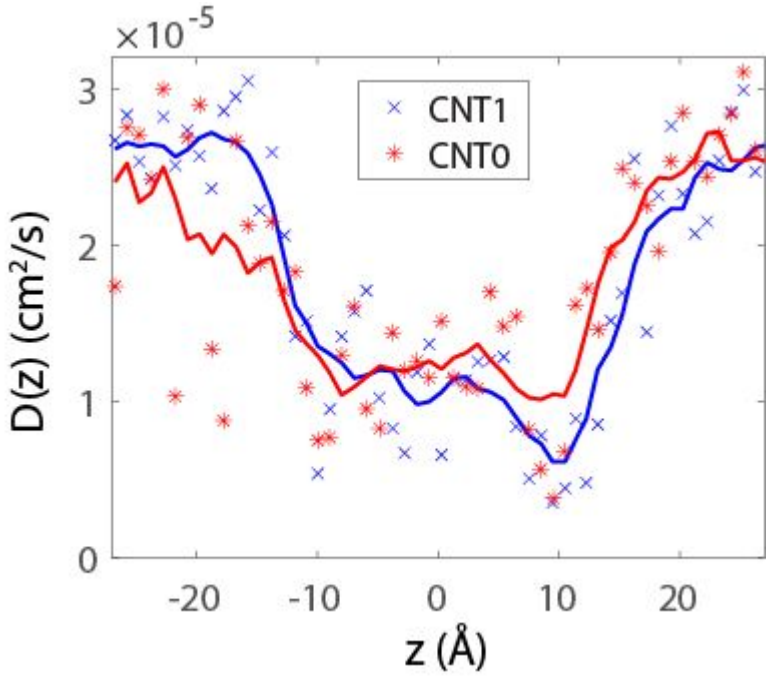

Figure 5. Position-dependent diffusion coefficients $D(z)$ calculated from umbrella sampling simulations (5 ns per window). The stars and crosses represent the estimated local diffusion coefficient at each window from the CNT0 and CNT1 simulations, respectively. The solid curves are the smoothed $D(z)$ profiles by applying a moving average over a stretch of 7 windows.

DISCUSSION

In this study, we demonstrated a new method to calculate the permeability of membrane channels, based on a one-dimensional free energy where the vertical position of a tagged solute is typically used as the reaction coordinate. The test on the CNT1 channel shows that our method provides reasonable predictions for the rate and the atomic details of the spontaneous crossings in long equilibrium simulations. For channels with much slower kinetics or at much lower solute concentrations, straightforward equilibrium simulations will become inefficient or infeasible to capture spontaneous crossing events, whereas our method could still be readily applied. Therefore, this method makes the calculation of single-channel permeability and conductance more convenient and reliable.

The simulation setups here are identical to those in the classical reactive flux method. Therefore, from these same simulations, we could also apply that method to calculate the rate. Specifically, from the correlation between the initial ion velocity at the barrier top and the final commitment of the ion in the unbiased trajectories, we calculated the transmission coefficient[12, 13], defined as the ratio of the transition rate to the ideal rate for ballistic barrier crossing as in the transition state theory. The calculated transmission coefficients are 0.18±0.17 for CNT0 and -0.15±0.17 for CNT1. With the very large relative statistical uncertainties here, the reactive flux method could only give a rough estimate for the upper bound of the transmission coefficient. In contrast, the transmission coefficients calculated from our method are 0.019±0.004 for CNT0 and 0.018±0.006 for CNT1, thus with a much higher statistical accuracy. Therefore, our method is clearly superior to the reactive flux method as it achieves significantly more accurate results with the same data and computational cost. The improvement arises from the fact that whereas

the reactive flux method takes only the initial velocity of each trajectory into the calculation, our method effectively averages over all the velocities[14, 15] when the dividing plane is crossed in a transition path, thus obtaining better statistics in the cases of multiple barrier re-crossings.

As formulated previously,[9] the crossing rate and single-channel permeability/conductance can also be calculated using a diffusion model. In principle, such a model assumes that the relaxation of orthogonal degrees of freedom is fast relative to the reaction coordinate. Also, the underlying Smoluchowski equation in the high friction limit is only valid for time scales in which the velocity autocorrelation function vanishes. Although the diffusion model also provides a good estimate of the permeability (see Results) for the relatively simple and rigid CNT channels here, a recent study[54] revealed that for some small molecules in lipid bilayers, the classical Smoluchowski equation is no longer valid due to subdiffusion behaviors. In contrast, although our method could efficiently handle diffusive barrier crossing, it is rigorous and is not contingent on the validity of diffusion model or the calculation of diffusion coefficients. Furthermore, our method does not require the reaction coordinate to be perfect. In fact, whereas the quality of the reaction coordinate can be evaluated by the fraction of the transition paths among the forward/backward trajectory pairs, it affects only the efficiency but not the correctness of the method.[17]

The kinetics of channel crossing can also be obtained by other methods that employ many short unbiased simulation trajectories. Notably, in the milestoning approach,[55, 56] the phase space is partitioned by boundaries called milestones, which, e.g., can be hyperplanes orthogonal to the chosen reaction coordinate. The kinetic information can then be obtained from unbiased trajectories initiated from one milestone and reaching another, assuming that the memory of the initial microstate has been lost. This approach is general and broadly applicable to both

equilibrium and non-equilibrium processes. In contrast, our method[17] is specifically designed for two-state barrier-crossing transitions and aims to predict the rate constants that are most relevant to experimental observables. Importantly, our method does not require the key assumption of loss of memory as in milestoning, which is not always trivially satisfied in complex systems.

The direct outcome of our method is the single-channel permeability for ion or uncharged solute at equilibrium. For ions, the equilibrium permeability also determines the single-channel conductance (Eq. 4) when the ionic current is linearly proportional to both the transmembrane voltage and the ion concentration. In contrast, to obtain the current I at a high voltage V beyond the linear range of the I-V curve, one will need to explicitly apply a voltage in the simulations[6] and evaluate the net ion flux across the channel. If such direct simulations are inefficient when the current is small and the crossing events are rare, our method[17] could similarly be applied to calculate the ion crossing rates and the flux under the applied voltage, as long as the single-ion conduction regime is still valid. In the presence of a voltage V, there will be a difference of eV between the baselines on the two sides of the free energy profile, and the forward and backward crossing rates will differ by a ratio of $\exp\left(\frac{eV}{k_BT}\right)$, with the net ion flux given by the difference between these two rates.

The channel crossings for the relatively simple CNTs in this study are typical two-state transitions, as the free energy (Fig. 2) features a single barrier only. For some complex membrane channels, in contrast, the free energy along the pore may have multiple valleys and barriers, and our method as well as the reactive flux method may have a problem because the solute could stay in some local free energy minima for a long time and a complete transition path would thus be very long. In such cases, it would be advisable to consider the complete channel

crossing as a sequence of multiple partial transition steps, each between two adjacent free energy minima as metastable states. With each step being a two-state transition, its forward and backward rates can be readily obtained by our method.[17] The overall crossing rate can then be calculated from all the stepwise transition rates. Sometimes, instead of using a single reaction coordinate as in this study, two- or three-dimensional (2D or 3D) free energies can be defined as a function of multiple descriptors of the solute or other degrees of freedom. If such a 2D or 3D free energy map has been sampled, it should be feasible either to further project it onto a 1D free energy along a single collective variable as the reaction coordinate, or to represent the solute crossing as multiple two-state transitions described above. In both cases our method[17] will be applicable to calculate the kinetic rates.

For the (8,8) CNTs used as the test case in this study, our calculations predict a picosiemens-conductance at a physiological KCl concentration, which is similar to the single-channel conductance[9] of some biological ion channels[41]. In this regard, other simulation studies[23, 57] indicated that the ion (Na^+, K^+) conductance depends sensitively on the size (diameter) of the CNT. Furthermore, given that charged functional groups are an important factor for the transport properties of CNTs,[24, 32] here we evaluated the effect of adding one carboxylate group to the (8,8) CNT. Our calculations showed that in comparison to the pristine CNT0, the functionalized CNT1 with a single COO^- group has only a slightly reduced free energy barrier (Fig. 2) and a slightly larger permeability/conductance for the K^+ ion (see Table 1). It appears that although the COO^- group increases the local K^+ concentration at the entrance, it does not have as much an influence on the free energy barrier located at the center of the CNT (see Fig. 2), which is the main determinant for the permeability. In contrast, an earlier work found that a ring of eight COO^- groups at the entrance of a (8,8) CNT does have a very significant effect on water and ion

permeation,[38] which may suggest that such effects are only prominent when the total charge of the functional groups is sufficiently large.

Ion conduction across individual CNTs or CNT membranes have also been measured in experiments.[24, 32-35, 58] Currently, MD simulations have not systematically reproduced the experimental results. In particular, a recent experimental study[42] reported that a narrow CNT (diameter 0.68 nm) has a single-channel conductance of ~69 pS at a KCl concentration of 1 M, which is even higher than the calculated conductance of the wider CNTs (diameter 1.08 nm) here. Most other MD studies[22, 25, 28, 57] also predicted very low conductance for CNTs with diameters less than 1.0 nm. The source of such discrepancy should be further investigated in future studies.

CONCLUSION

Our method presented here along with free energy calculations enables a rigorous and efficient calculation of the spontaneous solute crossing rate, which further determines the single-channel permeability and conductance, the major experimental observables for membrane channels. The method will thus quantitatively connect MD simulations and experiments.

ACKNOWLEDGEMENT

X.Z. was supported by the National Natural Science Foundation of China under Grants No. 11505156 and No.11875237 and the China Scholarship Council under Grant No. 201707260004.

References

1. Alberts, B.; Johnson, A.; Lewis, J.; Raff, M.; Roberts, K.; Walter, P., *Molecular Biology of the Cell*. 5th ed.; Garland Science: New York, 2008.
2. Liu, Y.; Zhu, F. Collective Diffusion Model for Ion Conduction through Microscopic Channels. *Biophys. J.* **2013,** 104, 368-376.
3. Roux, B.; Allen, T.; Berneche, S.; Im, W. Theoretical and Computational Models of Biological Ion Channels. *Q. Rev. Biophys.* **2004,** 37, 15-103.
4. Pothula, K. R.; Solano, C. J.; Kleinekathofer, U. Simulations of Outer Membrane Channels and Their Permeability. *Biochim. Biophys. Acta* **2016,** 1858, 1760-1771.
5. Kutzner, C.; Grubmüller, H.; de Groot, B. L.; Zachariae, U. Computational Electrophysiology: The Molecular Dynamics of Ion Channel Permeation and Selectivity in Atomistic Detail. *Biophys. J.* **2011,** 101, 809-817.
6. Gumbart, J.; Khalili-Araghi, F.; Sotomayor, M.; Roux, B. Constant Electric Field Simulations of the Membrane Potential Illustrated with Simple Systems. *Biochim. Biophys. Acta* **2012,** 1818, 294-302.
7. Khalili-Araghi, F.; Ziervogel, B.; Gumbart, J. C.; Roux, B. Molecular Dynamics Simulations of Membrane Proteins under Asymmetric Ionic Concentrations. *J. Gen. Physiol.* **2013,** 142, 465-475.
8. Hummer, G. Position-Dependent Diffusion Coefficients and Free Energies from Bayesian Analysis of Equilibrium and Replica Molecular Dynamics Simulations. *New J. Phys.* **2005,** 7, 34.
9. Zhu, F.; Hummer, G. Theory and Simulation of Ion Conduction in the Pentameric GLIC Channel. *J. Chem. Theory Comput.* **2012,** 8, 3759-3768.

10. Lee, C. T.; Comer, J.; Herndon, C.; Leung, N.; Pavlova, A.; Swift, R. V.; Tung, C.; Rowley, C. N.; Amaro, R. E.; Chipot, C.; Wang, Y.; Gumbart, J. C. Simulation-Based Approaches for Determining Membrane Permeability of Small Compounds. *J. Chem. Inf. Model.* **2016,** 56, 721-733.

11. Bennion, B. J.; Be, N. A.; McNerney, M. W.; Lao, V.; Carlson, E. M.; Valdez, C. A.; Malfatti, M. A.; Enright, H. A.; Nguyen, T. H.; Lightstone, F. C.; Carpenter, T. S. Predicting a Drug's Membrane Permeability: A Computational Model Validated with in Vitro Permeability Assay Data. *J. Phys. Chem. B* **2017,** 121, 5228-5237.

12. Frenkel, D.; Smit, B., *Understanding Molecular Simulation: From Algorithms to Applications*. 2 ed.; Academic Press: San Diego, 2002.

13. Roux, B.; Karplus, M. Ion-Transport in a Gramicidin-Like Channel - Dynamics and Mobility. *J. Phys. Chem.* **1991,** 95, 4856-4868.

14. Hummer, G. From Transition Paths to Transition States and Rate Coefficients. *J. Chem. Phys.* **2004,** 120, 516-523.

15. Best, R. B.; Hummer, G. Reaction Coordinates and Rates from Transition Paths. *Proc. Natl. Acad. Sci. U. S. A.* **2005,** 102, 6732-6737.

16. Daru, J.; Stirling, A. Divided Saddle Theory: A New Idea for Rate Constant Calculation. *J. Chem. Theory Comput.* **2014,** 10, 1121-1127.

17. Zhu, F. Calculating Transition Rates from Durations of Transition Paths. *J. Chem. Phys.* **2017,** 146, 124128.

18. Hummer, G.; Rasaiah, J. C.; Noworyta, J. P. Water Conduction through the Hydrophobic Channel of a Carbon Nanotube. *Nature* **2001,** 414, 188-190.

19. Zhu, F. Q.; Schulten, K. Water and Proton Conduction through Carbon Nanotubes as Models for Biological Channels. *Biophys J* **2003,** 85, 236-244.

20. Majumder, M.; Chopra, N.; Andrews, R.; Hinds, B. J. Nanoscale Hydrodynamics: Enhanced Flow in Carbon Nanotubes. *Nature* **2005,** 438, 44.

21. Lu, H. J.; Zhou, X. Y.; Wu, F. M.; Xu, Y. S. Effect of Charge on Water Filling/Emptying Transitions of Nanochannel. *J. Phys. Chem. B* **2008,** 112, 16777-16781.

22. Peter, C.; Hummer, G. Ion Transport through Membrane-Spanning Nanopores Studied by Molecular Dynamics Simulations and Continuum Electrostatics Calculations. *Biophys J* **2005,** 89, 2222-2234.

23. Song, C.; Corry, B. Intrinsic Ion Selectivity of Narrow Hydrophobic Pores. *J. Phys. Chem. B* **2009,** 113, 7642–7649.

24. Amiri, H.; Shepard, K. L.; Nuckolls, C.; Hernandez Sanchez, R. Single-Walled Carbon Nanotubes: Mimics of Biological Ion Channels. *Nano Lett.* **2017,** 17, 1204-1211.

25. Sumikama, T.; Saito, S.; Ohmine, I. Mechanism of Ion Permeation in a Model Channel: Free Energy Surface and Dynamics of K+ Ion Transport in an Anion-Doped Carbon Nanotube. *J. Phys. Chem. B* **2006,** 110, 20671-20677.

26. Das, R.; Ali, M. E.; Hamid, S. B. A.; Ramakrishna, S.; Chowdhury, Z. Z. Carbon Nanotube Membranes for Water Purification: A Bright Future in Water Desalination. *Desalination* **2014,** 336, 97-109.

27. Yang, H. Y.; Han, Z. J.; Yu, S. F.; Pey, K. L.; Ostrikov, K.; Karnik, R. Carbon Nanotube Membranes with Ultrahigh Specific Adsorption Capacity for Water Desalination and Purification. *Nat. Commun.* **2013,** 4, 2220.

28. Corry, B. Designing Carbon Nanotube Membranes for Efficient Water Desalination. *J. Phys. Chem. B* **2008,** 112, 1427-1434.

29. Rao, G. P.; Lu, C.; Su, F. Sorption of Divalent Metal Ions from Aqueous Solution by Carbon Nanotubes: A Review. *Sep. Purif. Technol.* **2007,** 58, 224-231.

30. Jae Hyun, P.; Susan, B. S.; Aluru, N. R. Ion Separation Using a Y-Junction Carbon Nanotube. *Nanotechnology* **2006,** 17, 895.

31. Choi, W.; Lee, C. Y.; Ham, M.-H.; Shimizu, S.; Strano, M. S. Dynamics of Simultaneous, Single Ion Transport through Two Single-Walled Carbon Nanotubes: Observation of a Three-State System. *J. Am. Chem. Soc.* **2011,** 133, 203-205.

32. Wu, J.; Gerstandt, K.; Zhang, H.; Liu, J.; Hinds, B. J. Electrophoretically Induced Aqueous Flow through Single-Walled Carbon Nanotube Membranes. *Nat. Nanotech.* **2012,** 7, 133-139.

33. Choi, W.; Ulissi, Z. W.; Shimizu, S. F. E.; Bellisario, D. O.; Ellison, M. D.; Strano, M. S. Diameter-Dependent Ion Transport through the Interior of Isolated Single-Walled Carbon Nanotubes. *Nat. Commun.* **2013,** 4, 2397.

34. Secchi, E.; Nigues, A.; Jubin, L.; Siria, A.; Bocquet, L. Scaling Behavior for Ionic Transport and Its Fluctuations in Individual Carbon Nanotubes. *Phys. Rev. Lett.* **2016,** 116, 154501.

35. Pang, P.; He, J.; Park, J. H.; Krstić, P. S.; Lindsay, S. Origin of Giant Ionic Currents in Carbon Nanotube Channels. *ACS Nano* **2011,** 5, 7277-7283.

36. Fornasiero, F.; In, J. B.; Kim, S.; Park, H. G.; Wang, Y.; Grigoropoulos, C. P.; Noy, A.; Bakajin, O. Ph-Tunable Ion Selectivity in Carbon Nanotube Pores. *Langmuir* **2010,** 26, 14848-14853.

37. Majumder, M.; Chopra, N.; Hinds, B. J. Effect of Tip Functionalization on Transport through Vertically Oriented Carbon Nanotube Membranes. *J. Am. Chem. Soc.* **2005,** 127, 9062-9070.

38. Corry, B. Water and Ion Transport through Functionalised Carbon Nanotubes: Implications for Desalination Technology. *Energy & Environmental Science* **2011,** 4, 751-759.

39. Chan, W. F.; Chen, H.; Surapathi, A.; Taylor, M. G.; Shao, X.; Marand, E.; Johnson, J. K. Zwitterion Functionalized Carbon Nanotube/Polyamide Nanocomposite Membranes for Water Desalination. *Acs Nano* **2013,** 7, 5308.

40. Fornasiero, F.; Park, H. G.; Holt, J. K.; Stadermann, M.; Grigoropoulos, C. P.; Noy, A.; Bakajin, O. Ion Exclusion by Sub-2-Nm Carbon Nanotube Pores. *Proc. Natl. Acad. Sci. U. S. A.* **2008,** 105, 17250-17255.

41. Bocquet, N.; Prado de Carvalho, L.; Cartaud, J.; Neyton, J.; Le Poupon, C.; Taly, A.; Grutter, T.; Changeux, J. P.; Corringer, P. J. A Prokaryotic Proton-Gated Ion Channel from the Nicotinic Acetylcholine Receptor Family. *Nature* **2007,** 445, 116-119.

42. Tunuguntla, R. H.; Henley, R. Y.; Yao, Y. C.; Pham, T. A.; Wanunu, M.; Noy, A. Enhanced Water Permeability and Tunable Ion Selectivity in Subnanometer Carbon Nanotube Porins. *Science* **2017,** 357, 792.

43. MacKerell, A. D.; Bashford, D.; Bellott, M.; Dunbrack, R. L.; Evanseck, J. D.; Field, M. J.; Fischer, S.; Gao, J.; Guo, H.; Ha, S.; Joseph-McCarthy, D.; Kuchnir, L.; Kuczera, K.; Lau, F. T. K.; Mattos, C.; Michnick, S.; Ngo, T.; Nguyen, D. T.; Prodhom, B.; Reiher, W. E.; Roux, B.; Schlenkrich, M.; Smith, J. C.; Stote, R.; Straub, J.; Watanabe, M.;

Wiórkiewicz-Kuczera, J.; Yin, D. All-Atom Empirical Potential for Molecular Modeling and Dynamics Studies of Proteins. *J. Phys. Chem. B* **1998,** 102, 3586.

44. Jorgensen, W. L.; Chandrasekhar, J.; Madura, J. D.; Impey, R. W.; Klein, M. L. Comparison of Simple Potential Functions for Simulating Liquid Water. *J. Chem. Phys.* **1983,** 79, 926.

45. Luo, Y.; Roux, B. Simulation of Osmotic Pressure in Concentrated Aqueous Salt Solutions. *J Phys Chem Lett* **2010,** 1, 183-189.

46. Comer, J.; Chen, R.; Poblete, H.; Vergara-Jaque, A.; Riviere, J. E. Predicting Adsorption Affinities of Small Molecules on Carbon Nanotubes Using Molecular Dynamics Simulation. *ACS Nano* **2015,** 9, 11761-11774.

47. Phillips, J. C.; Braun, R.; Wang, W.; Gumbart, J.; Tajkhorshid, E.; Villa, E.; Chipot, C.; Skeel, R. D.; Kale, L.; Schulten, K. Scalable Molecular Dynamics with Namd. *J. Comput. Chem.* **2005,** 26, 1781-1802.

48. Essmann, U.; Perera, L.; Berkowitz, M. L.; Darden, T.; Lee, H.; Pedersen, L. G. A Smooth Particle Mesh Ewald Method. *J. Chem. Phys.* **1995,** 103, 8577-8593.

49. Fukunishi, H. On the Hamiltonian Replica Exchange Method for Efficient Sampling of Biomolecular Systems: Application to Protein Structure Prediction. *J. Chem. Phys.* **2002,** 116, 9058-9067.

50. Zhu, F.; Hummer, G. Convergence and Error Estimation in Free Energy Calculations Using the Weighted Histogram Analysis Method. *J Comput Chem* **2012,** 33, 453-465.

51. Kumar, S.; Rosenberg, J.; Bouzida, D.; Swendsen, R.; Kollman, P. The Weighted Histogram Analysis Method for Free-Energy Calculations on Biomolecules. I. The Method. *J. Comput. Chem.* **1992,** 13, 1011-1021.

52. Dzubiella, J.; Allen, R. J.; Hansen, J. P. Electric Field-Controlled Water Permeation Coupled to Ion Transport through a Nanopore. *J. Chem. Phys.* **2004,** 120, 5001-5004.

53. Humphrey, W.; Dalke, A.; Schulten, K. Vmd: Visual Molecular Dynamics. *J. Mol. Graph.* **1996,** 14, 33-38.

54. Chipot, C.; Comer, J. Subdiffusion in Membrane Permeation of Small Molecules. *Sci Rep* **2016,** 6, 35913.

55. Faradjian, A. K.; Elber, R. Computing Time Scales from Reaction Coordinates by Milestoning. *J. Chem. Phys.* **2004,** 120, 10880-10889.

56. Elber, R. A New Paradigm for Atomically Detailed Simulations of Kinetics in Biophysical Systems. *Q. Rev. Biophys.* **2017,** 50, e8.

57. Samoylova, O. N.; Calixte, E. I.; Shuford, K. L. Molecular Dynamics Simulations of Ion Transport in Carbon Nanotube Channels. *J. Phys. Chem. C* **2015,** 119, 1659-1666.

58. Liu, H.; He, J.; Tang, J.; Liu, H.; Pang, P.; Cao, D.; Krstic, P.; Joseph, S.; Lindsay, S.; Nuckolls, C. Translocation of Single-Stranded DNA through Single-Walled Carbon Nanotubes. *Science* **2010,** 327, 64-67.

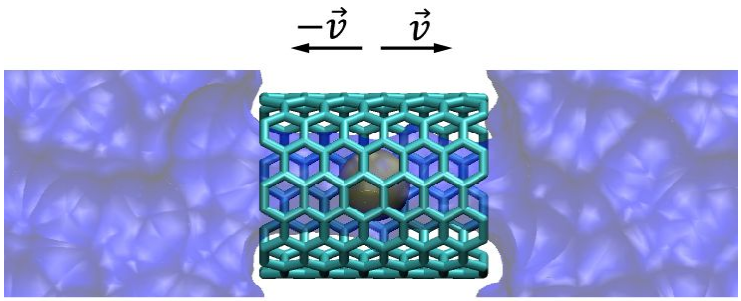

Single-channel permeability: $$p_s = \frac{1}{2}\langle\lambda(z_1, z_2)\rangle \cdot S \cdot \int_{z_1}^{z_2} e^{-G(z)/k_B T} dz$$